

X-RAY EMISSION FROM THE DOUBLE NEUTRON STAR BINARY B1534+12: POWERED BY THE PULSAR WIND?

O. KARGALTSEV, G. G. PAVLOV, AND G. P. GARMIRE

The Pennsylvania State University, 525 Davey Lab, University Park, PA 16802, USA

June 24, 2018

ABSTRACT

We report the detection of the double neutron star binary (DNSB) B1534+12 (= J1537+1155) with the *Chandra* X-ray Observatory. This DNSB ($P_{\text{orb}} = 10.1$ hr) consists of the millisecond (recycled) pulsar J1537+1155A ($P_A = 37.9$ ms) and a neutron star not detected in the radio. After the remarkable double pulsar binary J0737–3039, it is the only other DNSB detected in X-rays. We measured the flux of $(2.2 \pm 0.6) \times 10^{-15}$ ergs s⁻¹ cm⁻² in the 0.3–6 keV band. The small number of collected counts allows only crude estimates of spectral parameters. The power-law fit yields the photon index $\Gamma = 3.2 \pm 0.5$ and the unabsorbed 0.2–10 keV luminosity $L_X \approx 6 \times 10^{29}$ ergs s⁻¹ $\approx 3 \times 10^{-4} \dot{E}_A$, where \dot{E}_A is the spin-down power of J1537+1155A. Alternatively, the spectrum can be fitted by a blackbody model with $T \approx 2.2$ MK and the projected emitting area of $\sim 5 \times 10^3$ m². The distribution of photon arrival times over binary orbital phase shows a deficit of X-ray emission around apastron, which suggests that the emission is caused by interaction of the relativistic wind from J1537+1155A with its neutron star companion. We also reanalyzed the *Chandra* and *XMM-Newton* observations of J0737–3039 and found that its X-ray spectrum is similar to the spectrum of B1534+12, and its X-ray luminosity is about the same fraction of \dot{E}_A , which suggests similar X-ray emission mechanisms. However, the X-ray emission from J0737–3039 does not show orbital phase dependence. This difference can be explained by the smaller eccentricity of J0737–3039 or a smaller misalignment between the equatorial plane of the millisecond pulsar and the orbital plane of the binary.

Subject headings: pulsars: individual (PSR B1534+12 = PSR J1537+1155, PSR J0737–3039A, PSR J0737–3039B) — stars: neutron — X-rays: stars

1. INTRODUCTION

The sample of known double neutron star binaries (DNSBs) has nearly doubled over the last six years. Currently, eight such binaries are known (they are shown in the P - \dot{P} diagram in Fig. 1). All of them are found via radio timing of pulsars which provides binary orbital parameters, including the companion masses. DNSBs are thought to be formed in consequent supernova explosions in the course of evolution of massive binary systems. The details of binary evolution depend on initial star masses and binary orbital parameters (see Stairs 2004 for a review). It is generally believed that once the first neutron star (NS) is formed in the binary, accretion of matter from the evolved second star spins up the NS so that it becomes a millisecond (recycled) pulsar (MSP). Eventually, the second star explodes as a supernova and, if the explosion does not disrupt the binary or disintegrate the second star, a DNSB (or a NS-black hole binary) is formed.

Radio observations of DNSBs allow one to measure the masses of both NSs and test the predictions of General Relativity (GR). The recent discovery of the tight DNSB J0737–3039 ($P_{\text{orb}} = 2.45$ hours; see Burgay et al. 2003; Lyne et al. 2004; and Tables 1 and 2 for other details), where both NSs are radio pulsars orbiting in the plane seen nearly edge-on (the inclination angle i differs from 90° by $0^\circ 29 \pm 0^\circ 14$; Coles et al. 2005), dramatically boosted interest in DNSBs. Apart from measuring the GR parameters, the radio observations have shown

variations of the pulsed flux with orbital phase, for both pulsars. The radio pulse of the MSP J0737–3039A (hereafter J0737A) disappears around its superior conjunction¹, which has been interpreted as an eclipse of J0737A (Lyne et al. 2004), caused by synchrotron absorption in the magnetosphere of J0737B (Rafikov & Goldreich 2005; Lyutikov & Thompson 2005). Even more interesting is the finding that the generally faint pulsed radio emission of J0737B is strongly enhanced during two short orbital phase intervals of ~ 0.1 of the period around the phase of inferior conjunction of J0737B. These changes suggest that the magnetosphere of J0737B responds to the wind or radiation of the more energetic J0737A (Lyne et al. 2004; Jenet & Ransom 2004; Demorest et al. 2004; Zhang & Loeb 2004).

The J0737 was the first and, until this work, the only DNSB detected in X-rays. It has been observed with both *Chandra* (McLaughlin et al. 2004) and *XMM-Newton* (Campana, Possenti & Burgay 2004; Pellizzoni et al. 2004). Its luminosity is $L_X \sim (2-3) \times 10^{30}$ ergs s⁻¹ in the 0.2–10 keV band, assuming a 500 pc distance. The X-ray spectrum is rather soft; it can be fitted by either a power-law (PL) model with a photon index $\Gamma \sim 3-4$ or a blackbody (BB) model with $kT \approx 0.2$ keV and projected emitting area $A \sim 3 \times 10^4$ m². No X-ray variability has been reported for J0737 so far. A number of different interpretations of the X-ray emission have been suggested. These include emission from the surface and/or magnetosphere of J0737A (similar to solitary

¹ At the superior (inferior) conjunction of J0737A, it is located behind (in front of) J0737B along the observer's line-of-sight.

MSPs), emission from the J0737B’s magnetosphere (surface) energized (heated) by the J0737A’s wind (Zhang & Loeb 2004), and emission by particles accelerated in a bow shock produced by the J0737A’s wind in the interstellar medium (ISM) or in the magnetosphere of J0737B (Granot & Mészáros 2004). However, because of the small number of X-ray counts collected, it is difficult to discriminate between these models from observations of just one DNSB.

In this paper we report the detection of X-rays from the second DNSB, B1534+12 (=J1537+1155; hereafter J1537), discovered by Wolszczan (1991). One of the two NSs in this DNSB is a millisecond pulsar (J1537A hereafter; period $P_A = 37.9$ ms, characteristic age $\tau_A \equiv P_A/2\dot{P}_A = 248$ Myr, spin-down power $\dot{E}_A = 1.8 \times 10^{33}$ ergs s^{-1}) on a 10.1 hour eccentric ($e = 0.274$) orbit. As one can see from Figure 1 and Table 2, the J1537A’s parameters are generally close to those of J0737A, although J1537A is a factor of 3 less energetic. The dispersion measure of J1537A suggests a distance of about 0.7 kpc. The comparison of the observed orbital period decay with that predicted by GR allowed Stairs et al. (2002) to evaluate the distance more accurately: $D = 1.02 \pm 0.05$ kpc. Multi-year timing observations in the radio (Stairs et al. 2004) suggest that we are looking at J1537 close to its orbital plane ($i \simeq 77.2^\circ$), and J1537A is an almost orthogonal rotator (i.e., its magnetic axis and the line of sight are nearly orthogonal to the spin axis: $\alpha \approx 103^\circ$, $\zeta \approx 97^\circ$ at the epoch of our observation²) whose spin axis is misaligned with the orbital angular momentum by $\delta = 25^\circ \pm 4^\circ$ (Stairs et al. 2004; Thorsett et al. 2005). The second NS (hereafter J1537B) has not been detected as a radio pulsar, but its mass, $M_B = (1.345 \pm 0.001)M_\odot$, has been measured (Stairs et al. 2002). The detection of X-rays from J0737 prompted us to observe J1537, the second nearest DNSB. We describe the *Chandra* observation of J1537 in §2 and the observational results in §3, which also includes our reanalysis of the X-ray observations of J0737 and a comparison of the X-ray properties of these DNSBs. We discuss plausible X-ray emission models and compare their predictions with the observed X-ray properties in §4 and summarize our results in §5.

2. OBSERVATION

We observed J1537 with the Advanced CCD Imaging Spectrometer (ACIS) aboard *Chandra* on 2005 April 10 (start time 53,470.352222 MJD). The useful scientific exposure time was 36,080 s (first 935 s of the 37,015 s total exposure are excluded from the Good Time Intervals [GTIs]). The observation was carried out in Very Faint mode, and the pulsar was imaged on S3 chip of the ACIS-S array. The detector was operated in Full Frame mode which provides time resolution of 3.2 seconds. The data were reduced using the *Chandra* Interactive Analysis of Observations (CIAO) software (ver. 3.2.1; CALDB ver. 3.0.3).

3. X-RAY IMAGE AND SPECTRUM

Figure 2 shows the ACIS-S3 image of the J1537’s field. The X-ray source is clearly seen at R.A. = $15^{\text{h}}37^{\text{m}}09^{\text{s}}.986$, Decl. = $+11^\circ55'55''.39$ (the combined aspect determina-

² The angle ζ is changing with time, $d\zeta/dt \simeq -0.21^\circ/\text{yr}$ as a result of geodetic precession.

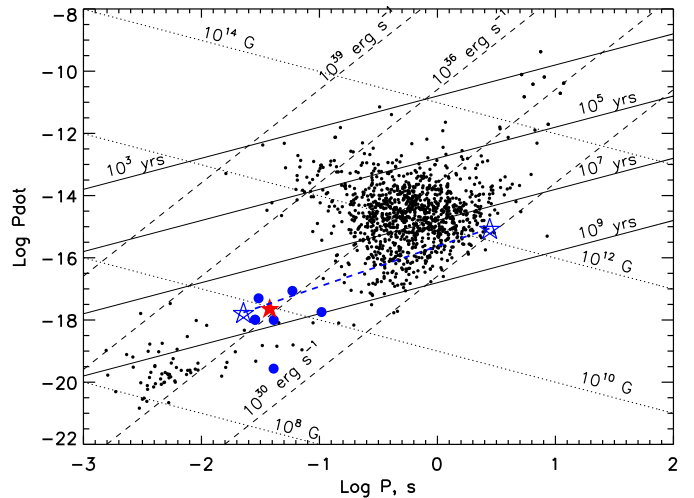


FIG. 1.— P - \dot{P} diagram for ≈ 1400 radio pulsars (small dots) from the ATNF catalog (Manchester et al. 2005). Lines of constant pulsar age, magnetic field, and \dot{E} are shown. Eight DNSBs are marked by different symbols. J1537A is marked by the filled star. The J0737 components are marked by open stars connected with the straight dashed line. The rest of the DNSBs are marked by filled circles. See the electronic edition of the *Journal* for the color version of this figure.

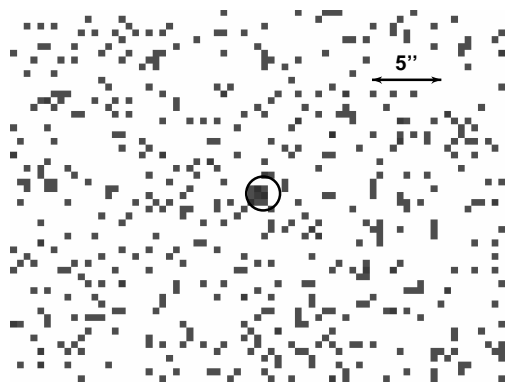


FIG. 2.— ACIS-S3 image of the J1537 field. The circle of $1''23$ radius shows the radio position of PSR J1537+1155 from Stairs et al. (2002).

tion and centroiding uncertainty is $0''.7$ at a 90% confidence level). Since this position is within $0''.5$ of the J1537A’s radio position (Stairs et al. 2002), we conclude with confidence that we detected the X-ray emission from J1537. The distribution of source counts in the ACIS image is consistent with that of a point source.

We extracted the pulsar spectrum from a circular aperture of 2.5 ACIS pixels radius ($= 1''.23$; $\approx 90\%$ encircled energy radius) using the CIAO `psextract` task. The background was extracted from a $5'' < r < 22''$ annulus centered on the source. The total number of counts within the source aperture is 16, of which 98.4% are expected to come from the source. The observed source flux is $(2.2 \pm 0.6) \times 10^{-15}$ erg s^{-1} cm^{-2} in the 0.3–6 keV range. We group the counts into 4 spectral bins, with each bin having 3–5 counts (see Fig. 3), and fit the spectrum with absorbed BB and PL models using the C-statistic (Cash 1979) implemented in XSPEC, ver. 11.3.0 (the fitting parameters are given in Table 3). To obtain constrained fits, we had to freeze the hydrogen column density, N_H . The pulsar’s dispersion measure, $DM = 11.6$ cm^{-3} pc, corresponds to $N_H = 3.6 \times 10^{20}$ cm^{-2} (assuming a 10% ISM ionization). This value is close to the

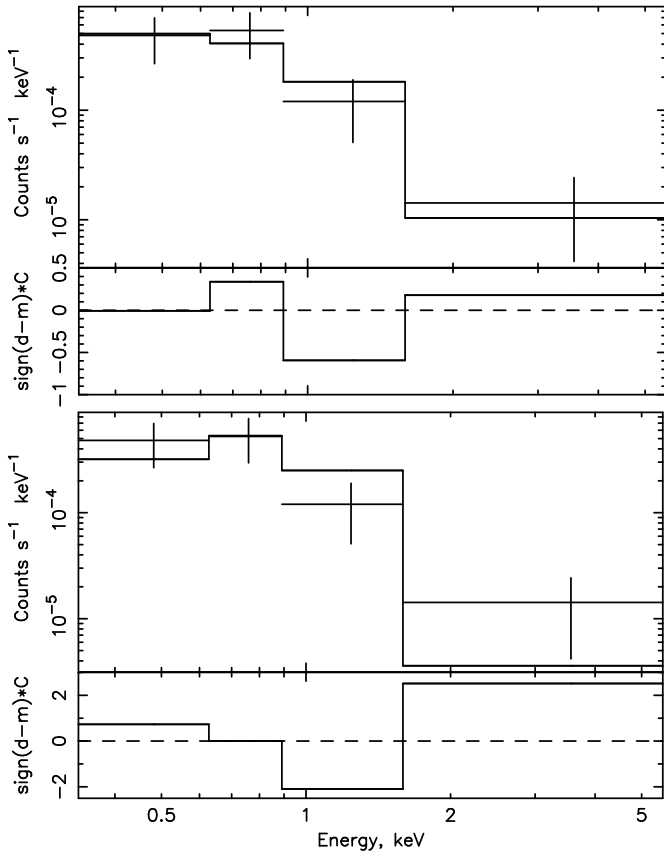


FIG. 3.— X-ray spectrum of J1537 fitted with PL (*top*) and BB (*bottom*) models. The contributions of the energy bins into the best-fit C-statistic are shown in lower panels, multiplied by -1 when the number of data counts is smaller than the number of model counts.

total Galactic absorption in neutral hydrogen, $3.6 \times 10^{20} \text{ cm}^{-2}$ (Dickey & Lockman 1990) in the direction of J1537 ($l = 19^\circ 85$, $b = 48^\circ 34$), which is located well above the Galactic plane ($z = 0.76$ kpc at the distance of 1 kpc). Therefore, we adopt $N_{\text{H}} = 3.6 \times 10^{20} \text{ cm}^{-2}$ in the X-ray fits.

The spectrum fits a soft PL with a photon index $\Gamma = 2.7\text{--}3.7$ and an isotropic unabsorbed 0.2–10 keV luminosity $L_{\text{X}} \equiv 4\pi D^2 F_{\text{X}}^{\text{unabs}} \simeq (6.1_{-2.1}^{+3.0}) \times 10^{29} \text{ ergs s}^{-1}$ at $D = 1$ kpc. The temperature and the projected area of the emitting region obtained from the BB fit are strongly correlated (see Fig. 4), which results in large uncertainty of these parameters. The BB model gives the best-fit temperature $T_{\text{BB}} = 2.2$ MK and a projected emitting area $A = 5 \times 10^3 \text{ m}^2$. The projected area is much smaller than that of a NS, $\sim 3 \times 10^8 \text{ m}^2$, suggesting that the thermal radiation might be emitted from small, hot polar caps with an effective radius $R \sim 39(\cos\zeta)^{-1/2} \text{ m}$ and a bolometric luminosity $L_{\text{bol}} = \sigma T^4 A (\cos\zeta)^{-1} = (6.8 \pm 2.1) \times 10^{28} (\cos\zeta)^{-1} \text{ ergs s}^{-1}$, where $\langle \cos\zeta \rangle$ is the time-averaged cosine of the angle between the line of sight and the normal to the visible polar cap ($\langle \cos\zeta \rangle \approx 0.62$ for the axis orientations suggested by Stairs et al. 2004, assuming a centered dipole with two equivalent polar caps and neglecting the GR bending of photon trajectories). The X-ray luminosity of J1537 corresponds to $3.4 \times 10^{-4} \dot{E}_A$ and $3.8 \times 10^{-5} (\cos\zeta)^{-1} \dot{E}_A = 6.1 \times 10^{-5} \dot{E}$ for the PL (0.2–10

keV band) and BB fits, respectively. The scarce statistics does not allow us to discriminate between the BB and PL models.

To compare the spectra and light curves of J1537 and J0737, we reanalyzed the *Chandra* ACIS and *XMM-Newton* EPIC observations of J0737, using the same spectral models and the same approach to the data analysis as for J1537. The observations have been described by McLaughlin et al. (2004), Campana et al. (2004), and Pellizzoni et al. (2004). The results of our fits are presented in Table 3 and Figure 5. For the PL fit of the ACIS spectrum, we obtained about the same parameters as McLaughlin et al. (these authors did not fit the BB model). As for the EPIC data, we found, in accordance with Campana et al., that the EPIC-pn data are too noisy for a useful analysis because of the very high background in the timing mode. Therefore, we only used the MOS1 and MOS2 data. For each of the MOS detectors, we created a light curve with binning time of 10 s and constructed GTIs excluding the time intervals during which the total chip count rate exceeded 3 counts s^{-1} (the remaining useful time is 24.62 and 24.60 ks for MOS1 and MOS2, respectively). The spectra we extracted from circular apertures of $46''$ radius ($\simeq 90\%$ encircled energy). Comparing the properties of the X-ray radiation from J0737 and J1537, we see that the spectral parameters are very similar: $\Gamma \approx 3$ for the PL fit, and $kT \approx 0.2$ keV for the BB fit.

In the upper panel of Figure 6 we show the distribution of arrival times for the 16 detected photons over binary orbital phases of J1537 ($\phi_{\text{orb}} = 0$ corresponds to periastron passage)³. Notice that no events arrived during the 12,795 s interval between MJD 53470.46046 and 53470.60855, which corresponds to the phase interval $[0.365; 0.717]$ ($\Delta\phi_{\text{orb}} = 0.352$). This interval includes the phase of apastron, $\phi = 0.5$, and the phase of superior conjunction of J0537A, $\phi = 0.408$ at the epoch of our *Chandra* observation. The probability of getting zero counts by chance in the 12,795 s interval is 0.0034 (assuming Poisson statistics), i.e. the observed “gap” has a $\approx 3\sigma$ significance. For comparison, we plotted similar distributions for the *Chandra* and *XMM-Newton* observations of J0737 (middle and bottom panels of Fig. 6), which do not show a statistically significant dependence on orbital phase (Fig. 7).

4. DISCUSSION.

The small number of detected counts does not allow one to determine the nature of the X-ray emission from J1537 unequivocally. Among viable models are intrinsic emission from the surface or magnetosphere of the NS(s) (just as in solitary pulsars), the synchrotron emission resulting from the interaction between the pulsar winds or between the wind of J1537A and the magnetosphere of J1537B, and emission from the inner magnetosphere or surface of J1537B triggered by the relativistic particles from the J1537A’s wind. Below we briefly discuss these interpretations, with emphasis on different dependences of the X-ray flux on binary phase.

³ To calculate the event orbital phases, we used the binary ephemeris for the epoch of our observation kindly provided by Ingrid Stairs: $P_{\text{orb}} = 0.420737299122$ days, epoch of periastron 53470.309046790 MJD, longitude of periastron $290^\circ.004585816$.

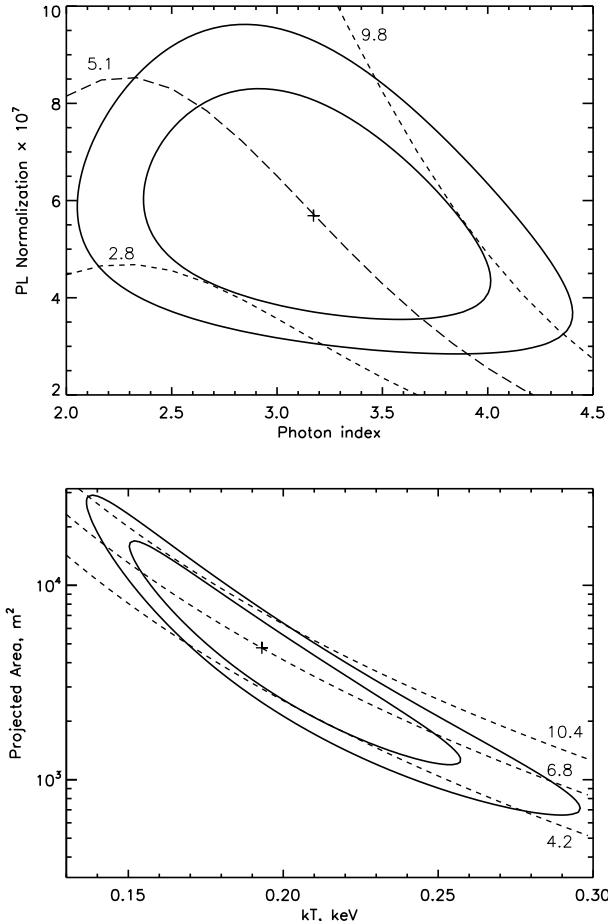


FIG. 4.— Confidence contours (68% and 90%) for the PL (*top*) and BB (*bottom*) fits to the spectrum of J1537. The PL normalization is in units of 10^{-7} photons $\text{cm}^{-2} \text{s}^{-1} \text{keV}^{-1}$ at 1 keV. The BB normalization (vertical axis) is the projected emitting area in units of m^2 , for $D = 1$ kpc. The lines of constant unabsorbed flux (top panel; in units of 10^{-15} ergs $\text{cm}^{-2} \text{s}^{-1}$, in 0.2–10 keV band) and constant $L_{\text{bol}}(\cos \zeta)$ (bottom panel; in units of 10^{28} ergs s^{-1}) are plotted as dashed lines, for fixed $N_{\text{H}} = 3.6 \times 10^{20} \text{cm}^{-2}$.

4.1. Phase-dependent X-ray emission powered by the wind from pulsar A

The apparent lack of J1537’s X-ray emission near the apastron suggests that a phase-dependent interaction mechanism is responsible for the X-ray emission in close DNSBs. The interaction can proceed via several different mechanisms, and the *pulsar winds* are expected to play an important role in each of them. Below we consider plausible scenarios.

4.1.1. Interaction of pulsar A’s wind with the outer magnetosphere of pulsar B

As discussed in many papers on pulsars in binaries (e.g., Arons & Tavani 1993), phase-dependent synchrotron emission can be produced when the pulsar’s wind collides with the wind or magnetosphere of the secondary companion. For a DNSB, the position of the interaction site (e.g., of the bow-shock head) on the line connecting the two pulsars can be estimated by balancing the pressure of the pulsar A’s wind with the pressure

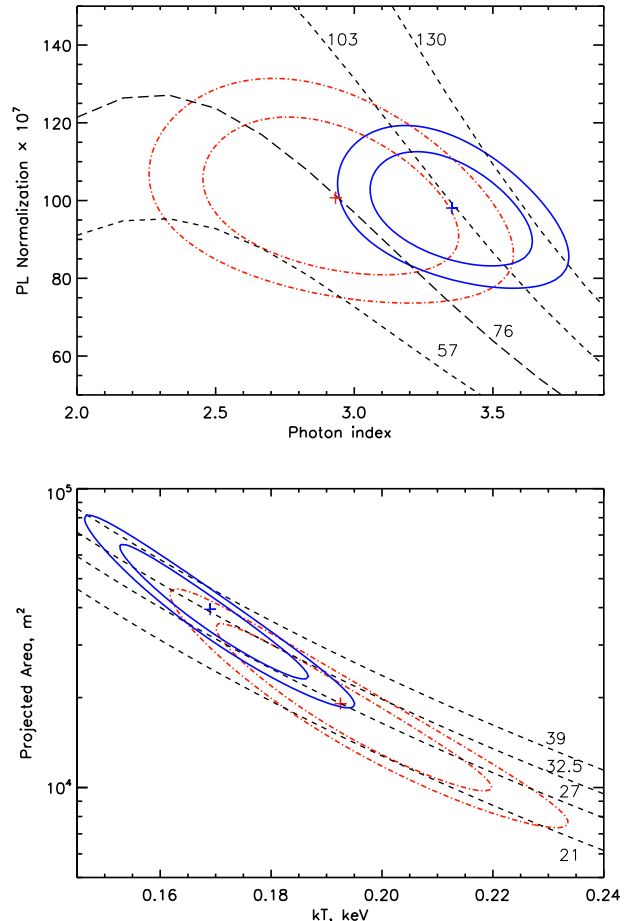


FIG. 5.— Same as in Fig. 4 but for J0737. Solid and dash-dotted contours are from the XMM-Newton EPIC MOS and Chandra ACIS observations, respectively. See the electronic edition of the Journal for the color version of this figure.

of pulsar B’s wind or magnetosphere:

$$\frac{\dot{E}_A f_A}{4\pi c (d_{AB} - r_B)^2 c} \approx \frac{\dot{E}_B}{4\pi c r_B^2} \begin{cases} f_B & \text{if } r_B \gg R_{lc,B} \\ g_B \left(\frac{R_{lc,B}}{r_B}\right)^4 & \text{if } r_B \ll R_{lc,B} \end{cases} \quad (1)$$

where d_{AB} is the distance between the binary companions, r_B is the distance between the interaction site and pulsar B, and $R_{lc,B} = 4.8 \times 10^9 P_B$ cm is the light cylinder radius for pulsar B (approximately equal to the size of undisturbed magnetosphere). The factors f_A and f_B take into account possible anisotropy of the pulsar winds ($f = 1$ for an isotropic wind). They depend on the colatitudes, ϑ_A and ϑ_B , of the wind interaction site with respect to the A’s and B’s spin axes because the pulsar wind should be axially symmetric; for instance, $f = (3/2) \sin^2 \vartheta$ for an angular distribution similar to that of magnetic dipole radiation (cf. Arons et al. 2004), or

$$f = \begin{cases} (\sin \Delta)^{-1} & \text{if } |\vartheta - \pi/2| < \Delta \\ 0 & \text{otherwise} \end{cases} \quad (2)$$

for an equatorial outflow with a uniform energy flux within sharp boundaries. The factor $g_B = (3/4)(1 + 3 \cos^2 \Theta_B)$ takes into account the dependence of the magnetic pressure on the polar angle Θ_B with respect to the B’s magnetic axis.

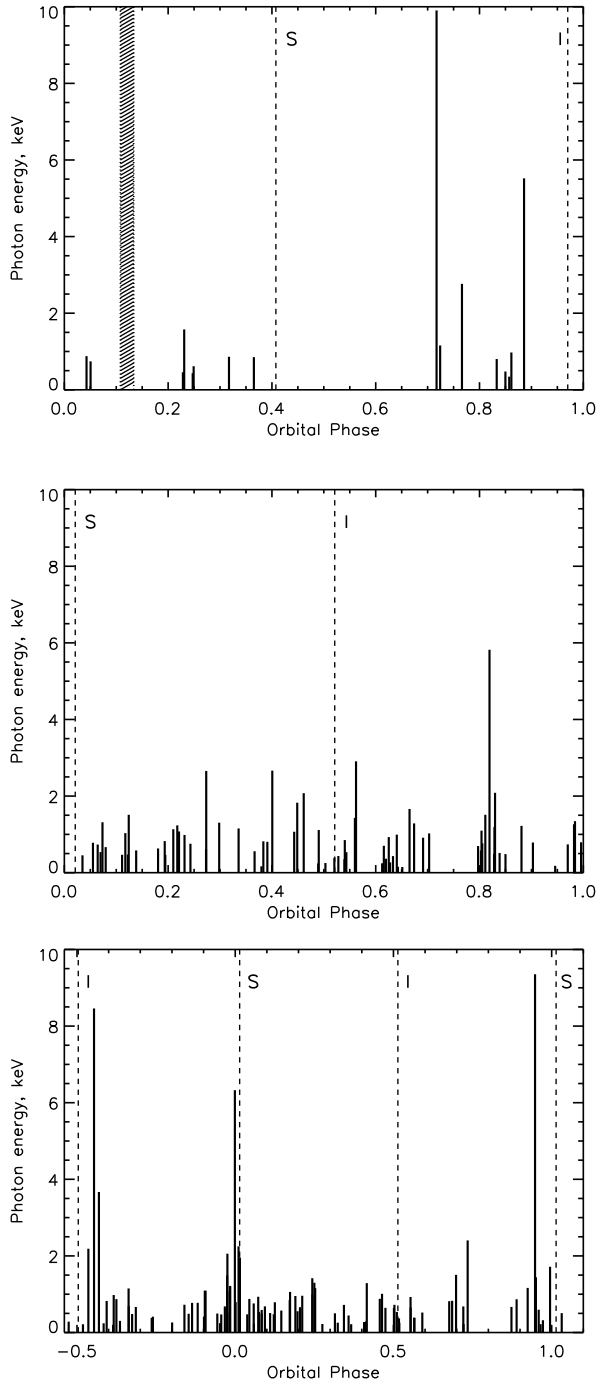


FIG. 6.— Distributions of photon arrival times over binary phase for the *Chandra* ACIS observations of J1537 (*top*) and J0737 (*middle*), and for the *XMM-Newton* MOS1 and MOS2 observation of J0737 (*bottom*). Zero phase corresponds to periastron passage. Only first 14.05 ks of the *XMM-Newton* exposure, least affected by the flare background, are used here. The hatched area in the top panel shows the time interval excluded from the GTIs. The dashed vertical lines show the phases of superior (S) and inferior (I) conjunctions for J1537A and J0737A at the epochs of the *Chandra* and *XMM-Newton* observations.

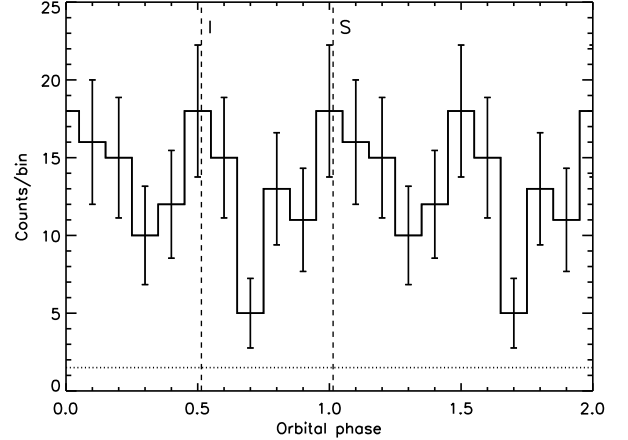


FIG. 7.— X-ray light curve of J0737 folded with the binary period. We used both *Chandra* ACIS and *XMM-Newton* MOS data taken over the length of a single binary revolution in each case (most of the remaining 51-ks-long *XMM-Newton* exposure suffered from strong background flares.). The horizontal dotted line shows the background level.

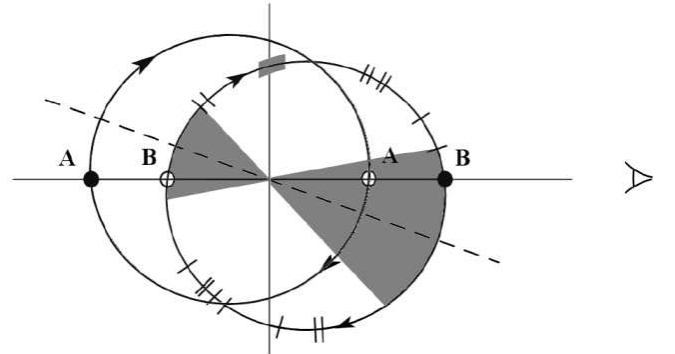


FIG. 8.— Configuration of the J1537 binary at the epoch of the *Chandra* observation (53,470 MJD). View from above the orbital plane with the Earth to the right is shown. The ellipses show the orbits of J1537A and J1537B around the center of mass of the system. The filled and open circles show the positions of the components at superior and inferior conjunction of J1537A. The vertical solid line is the line of nodes, and the dashed straight line is the apsidal line. The ticks on the J1537B's orbit show the distribution of the 16 detected photons over the orbit, while the shaded part of the orbit (around the line of nodes) corresponds to the excluded time interval at the beginning of the observation. (Notice that the distribution of photons over the orbit looks different from that over phases in Fig. 6 because of the substantial eccentricity; in particular, the gap near the periastron is much larger because of the increased orbital velocity.) The shaded sectors show the ranges of true anomalies θ (counted clockwise from periastron) in which the lack of detected photons could be explained by a misalignment of the A's spin axis and the binary angular momentum, assuming an equatorial outflow of the A's wind (see §4.1.1).

Since B is expected to be a slowly rotating, old (perhaps even dead) pulsar, we can assume $\dot{E}_B \ll \dot{E}_A$ (e.g., $\dot{E}_B/\dot{E}_A = 2.8 \times 10^{-4}$ for J0737), which gives

$$r_B \sim \begin{cases} d_{AB}(\dot{E}_B f_B / \dot{E}_A f_A)^{1/2} & \text{for } r_B > R_{lc,B} \\ d_{AB}^{1/3} R_{lc,B}^{2/3} (\dot{E}_B g_B / \dot{E}_A f_A)^{1/6} & \text{for } r_B < R_{lc,B} \end{cases} \quad (3)$$

The interaction may occur outside or inside the B's light cylinder, depending on the separation and the unknown properties of pulsar B. In particular, $r_B < R_{lc,B}$ (i.e., the B's magnetosphere is compressed by the A's wind on

the “dayside”) if

$$P_B > 0.66 d_{AB,11} (\dot{E}_{B,30} g_B / \dot{E}_{A,33} f_A)^{1/2} \text{ s}, \quad (4)$$

which corresponds to

$$P_B > \begin{cases} 0.3 (g_B / f_A)^{1/2} \text{ s} & \text{for J0737} \\ 1.1 (d_{AB}/a) (\dot{E}_{B,30} g_B / f_A)^{1/2} \text{ s} & \text{for J1537} \end{cases}, \quad (5)$$

where a is the semimajor axis of the binary relative orbit ($a = 2.28 \times 10^{11}$ cm and 8.78×10^{10} cm for J1537 and J0737, respectively).

The shocked A’s wind can generate synchrotron X-ray emission if the wind particles are sufficiently energetic and the magnetic field B is strong enough in the emission region:

$$\gamma^2 B \gtrsim 10^{12} (E/5 \text{ keV}), \quad (6)$$

where γ is the Lorentz factor, and E is the photon energy. For the plausible case $r_B < R_{lc,B}$, the magnetic field at the interaction site can be estimated from the pressure balance between the A’s wind and the B’s magnetic pressure:

$$B = \left(\frac{2\dot{E}_A f_A}{cd_{AB}^2} \right)^{1/2} = \frac{a}{d_{AB}} f_A^{1/2} \begin{cases} 7.1 \text{ G} & \text{for J0737} \\ 1.5 \text{ G} & \text{for J1537} \end{cases}. \quad (7)$$

At such fields, we need electrons with Lorentz factors $\gtrsim 10^5$ – 10^6 to produce synchrotron X-rays. The recent pulsar wind models (e.g., Kirk & Skjæraasen 2003 and references therein) suggest that the initially Poynting-flux-dominated wind of pulsar A converts most of its electromagnetic energy into particle kinetic energy at a distance much greater than the binary separation, which implies that the bulk Lorentz factor upstream of the interaction site remains the same as acquired in the pulsar A’s magnetosphere. Although the predictions of the current pulsar models are rather uncertain in this regard (in particular, the Lorentz factor depends on poorly known “multiplicity” of the pair cascades; e.g., Hibschan & Arons 2001), the required values of γ are likely too large to be produced in the A’s magnetosphere, which means that additional acceleration must occur at the interaction site (e.g., caused by reconnection of the magnetic fields of the A’s wind and B’s magnetosphere, similar to the magnetic reconnection at the interaction of the solar wind with the Earth’s magnetosphere).

If the shocked/accelerated A’s wind is the sole source of the X-ray emission, the X-ray luminosity should be a fraction of the A’s wind power:

$$L_X = \epsilon_\Omega \epsilon_e \epsilon_{\text{rad}} \epsilon_X \dot{E}_A \quad (8)$$

where $\epsilon_\Omega \approx f_A (r_\perp / 2d_{AB})^2$ is the fraction of A’s power intercepted by the B’s magnetosphere with a transverse size r_\perp that depends on geometry of the interaction region (crudely, $r_\perp \sim R_{lc,B}$), ϵ_e is the fraction of energy of the shocked/accelerated wind carried by particles (electrons and/or positrons), $\epsilon_{\text{rad}} \approx \min(1; t_{\text{flow}}/t_{\text{rad}})$ is the radiative efficiency, i.e. the fraction of intercepted energy emitted as (synchrotron) radiation (t_{rad} and t_{flow} are the time of synchrotron losses and the flow time in the emission region), and ϵ_X is the fraction of synchrotron power emitted in the X-ray range. The intercepted fraction can be estimated as $\epsilon_\Omega \sim 6 \times 10^{-3} f_A (r_\perp / R_{lc,B})^2$ and $\sim 5 \times 10^{-4} f_A (r_\perp / 10^{10} \text{ cm})^2 (a/d_{AB})^2$ for J0737 and

J1537, respectively. The fraction ϵ_e depends on acceleration mechanism (e.g., magnetic reconnection); the latter is currently unknown, but the assumption that ϵ_e is not much lower than unity seems plausible. The fraction ϵ_{rad} depends on the particle energy spectrum, geometry of emitting region, and flow velocity. For a particle of given energy, the time of synchrotron losses is $\tau_{\text{rad}} = 510 \gamma_6^{-1} B^{-2} \text{ s}$, while the flow time is $t_{\text{flow}} \sim l/v_{\text{flow}} \sim 0.3 l_{10} \beta^{-1} \text{ s}$, where $l = 10^{10} l_{10} \text{ cm}$ is the travel length, and $\beta = v_{\text{flow}}/c$. This gives $\epsilon_{\text{rad}} \sim \min(1; 7 \times 10^{-4} l_{10} \gamma_6 B^2 \beta^{-1})$. We see that electrons emit a very small fraction of their energy unless the travel length substantially exceeds a typical size of the B’s magnetosphere. Finally, the fraction ϵ_X cannot be reliably estimated without knowing the particle energy distribution. However, even for ϵ_X (and ϵ_e) close to unity, the above estimates of ϵ_Ω and ϵ_{rad} suggest the A’s wind should be substantially anisotropic ($f_A \gg 1$) and/or the emitting particles should spend a long time ($\gtrsim 10^2 \text{ s}$) in the emitting region to explain the ratio $L_X/\dot{E}_A \sim 3 \times 10^{-4}$ observed⁴ in J0737 and J1537.

The interaction mechanism and the properties of the A’s wind can be inferred from the analysis of the dependence of the X-ray emission on orbital phase. The collision of the A’s wind with the B’s magnetosphere is expected to form a bow-shock, convex toward pulsar A, with the shocked A’s wind flowing in a magnetosheath engulfing the B’s magnetosphere (Arons et al. 2004; Lyutikov 2004). It is tempting to explain the X-rays observed from J0737 and J1537 as synchrotron emission from the shocked A’s wind in the magnetosheath (as discussed by Granot & Mészáros 2004). Such an explanation implies an orbital dependence of the X-ray flux caused by the relativistic beaming (Doppler boost), showing a minimum flux at the phase of inferior conjunction of pulsar A, when the wind in the sheath is flowing away from the observer, and a maximum flux around the superior conjunction. For a reasonable flow speed, $v_{\text{flow}} = \beta c$, the Doppler boost modulation can be quite large, up to $F_{\text{max}}/F_{\text{min}} = [(1 + \beta)/(1 - \beta)]^{\Gamma+2}$, especially at the observed large photon index, $\Gamma \sim 3$. However, the observed distributions of photons over orbital phase do not show a statistically significant flux deficit at the phase of A’s inferior conjunction, in neither J0737 nor J1537 (see Figs. 6 and 7). Therefore, such an explanation can be ruled out. It seems surprising that no orbital modulation caused by the anisotropy of the flow in the putative magnetosheath is seen (unless, of course, our assumption, that the X-rays are produced by interaction of the A’s wind with the B’s magnetosphere, is wrong). We can only speculate that either the magnetosheath does not form because the A’s wind is strongly magnetized or the X-ray emitting particles accelerated by magnetic reconnection do not flow into the magnetosheath.

Having ruled out the magnetosheath as the source of the observed X-rays, we can, nevertheless, suggest two explanations for the observed orbital dependence of X-ray emission in J1537, such that they do not contradict to the lack of such dependence in J0737. First, this difference may be connected with the fact that J1537 has a

⁴ We should note that the L_X estimates in §3 are based on the assumption of isotropic X-ray emission, which is not necessarily true; the actual L_X can be lower or higher than estimated.

substantial eccentricity while J0737 is on an almost circular orbit. At apastron, the separation d_{AB} is larger than at periastron by a factor $(1+e)/(1-e)$, which is 1.755 for J1537, vs. 1.192 for J0737. The decrease of the magnetic field and particle number density, n_e , at the interaction site with increasing separation should lead to a lower X-ray luminosity at apastron in eccentric DNSBs. Crudely, assuming ϵ_X does not depend on d_{AB} substantially, the luminosity behaves as $L_X \sim \epsilon_X n_e V \mathcal{P}_{\text{syn}} \propto V d_{AB}^{-4}$, where $\mathcal{P}_{\text{syn}} \propto B^2 \propto d_{AB}^{-2}$ is the total synchrotron power per electron, and V is the emission volume. The dependence of the latter on d_{AB} is rather uncertain, but it seems reasonable to assume $V \propto r_B^3$. Under this assumption, we obtain $V \propto d_{AB}^3$ or $V \propto d_{AB}$ for $r_B > R_{lc,B}$ or $r_B < R_{lc,B}$, respectively, so the increase of V with d_{AB} does not compensate for the decrease caused by decreasing B and n_e . In particular, $L_X \propto d_{AB}^{-3}$ for $r_B < R_{lc,B}$, which means that we can expect the luminosity at apastron to be a factor of 5.4 lower than at periastron, for J1537. Although the effect of varying binary separation can explain the observed deficit around apastron in J1537, we do not see an increased count rate at periastron, predicted by this model; however, we cannot rule it out because of the scarce statistics of our data.

In addition to the varying binary separation, the phase dependence of the X-ray flux in J1537 can be caused by a misalignment between the binary orbital plane and the equatorial plane of pulsar A, where most of the A's wind is expected to be confined. In this case, one should expect brighter X-ray emission at orbital phases when pulsar B plunges in the dense wind flowing in the equatorial plane of pulsar A. For instance, if the equatorial outflow is confined between two conical surfaces, within an angle $\pm\Delta$ from the equatorial plane, and the A's spin axis is inclined at an angle δ to the direction of the orbital angular momentum, then, at $\delta > \Delta$, the wind ‘‘misses’’ pulsar B in two segments of the orbit: $|\psi| < \eta$ and $|\pi - \psi| < \eta$, where ψ is the azimuthal angle counted from the projection of the A's spin onto the orbital plane, and η is given by the equation

$$\cot \eta = \tan \Delta (\tan^2 \delta - \tan^2 \Delta)^{-1/2} (\cos \delta)^{-1}. \quad (9)$$

In other words, one should expect a photon deficit in two phase intervals corresponding to two sectors symmetric with respect to the A's spin projection onto the orbital plane. If such a phase dependence is observed, then η can be measured, and Δ can be found from the equation

$$\tan^2 \Delta = \cot^2 \eta \sin^2 \delta (1 + \cot^2 \eta \cos^2 \delta)^{-1}. \quad (10)$$

For J1537, we determined the true anomaly θ for each of the 16 events and marked the events on the J1537B orbit in Figure 8. Because of the higher (lower) NS velocities near the periastron (apastron), a relatively small phase segment around $\phi = 0$ with no photons detected, $-0.114 < \phi < 0.043$, translates into a sector of true anomalies, $-68^\circ < \theta < 28^\circ$, whose width, $\Delta\theta_{\text{per}} = 95^\circ$, is even larger than that of the photon-free sector at apastron, $\Delta\theta_{\text{ap}} = 80^\circ$ ($150^\circ < \theta < 231^\circ$). If we interpret the photon deficit in these sectors as caused by the anisotropy of the wind outflow, then, from the symmetry requirement, the sectors in which the J1537A's wind misses J1537B (shaded in Fig. 8) are $-30^\circ < \theta < 28^\circ$ and $150^\circ < \theta < 208^\circ$, i.e., the projection of the A's spin onto the orbital plane almost coincides with the apsidal

line, and $\eta \leq 29^\circ$. Since $\delta = 25^\circ \pm 4^\circ$ for J1537 (Stairs et al. 2002), equation (10) gives a lower limit on the half-opening angle of the equatorial outflow, $\Delta \geq 18^\circ - 25^\circ$. Being consistent with the observed phase dependence, such an explanation is also attractive because it implies an increased particle and energy supply in the two segments of orbit where the J1537A's wind encounters J1537B (f_A can be as large as 2.4–3.2, according to eq. [2]), a higher magnetic field at the interaction region (by a factor of $f_A^{1/2}$), and, correspondingly, a smaller ratio $t_{\text{flow}}/t_{\text{rad}}$ (by a factor of f_A). These consequences of the wind anisotropy alleviate the energetic and geometric restrictions inherent in the interpretation of the X-ray emission as caused by the interaction of the A's wind with the B's magnetosphere. We should emphasize, however, that the X-ray flux deficit around periastron is not statistically significant, and this hypothesis can be confirmed only by a deeper observation. For J0737, the angle δ is rather uncertain ($0 < \delta < 60^\circ$; Manchester et al. 2005), so one can assume that the lack of a clear orbital phase dependence means that $\delta < \Delta$, i.e., the J0737A's wind interacts with J0737B throughout the whole orbit.

In addition to the energetics and geometry (luminosity and its phase dependence), some information on the interaction mechanism can be obtained from the X-ray spectra. In this regard, we should note that the spectra observed in J1537 and J0737 are surprisingly soft ($\Gamma \sim 3$) in comparison with, e.g., the spectra observed in pulsar wind nebulae ($\Gamma \sim 1-2$). The models of particle acceleration by ultrarelativistic MHD shocks also suggest much flatter spectra, $\Gamma \simeq 1.6$, corresponding to the slope $p \simeq 2.2$ of the particle energy spectrum (Achterberg et al. 2001). We can speculate, however, that acceleration via relativistic magnetic reconnection might produce softer spectra. Also, we do not exclude the possibility that the observed spectra consist of two components: a hard PL component from the shocked wind and a soft thermal component from the polar caps of pulsar A (see §4.2).

4.1.2. Emission from B's inner magnetosphere and/or surface induced by captured A's wind

There is a possibility that some fraction of the A's wind is captured by the B's magnetosphere (e.g., similar to capturing solar wind in the Earth magnetosphere). The captured wind can increase the magnetospheric pair density or even precipitate onto the NS surface (such a possibility has been discussed by Zhang & Loeb 2004 to explain the flaring radio emission of J0737B). The captured relativistic particles lose a substantial fraction of their energy to synchrotron and inverse Compton radiation, thereby increasing the radiative efficiency, ϵ_{rad} , of the intercepted wind. The particles traveling along the open field lines may reach the NS polar caps and heat them to X-ray temperatures, up to a few million kelvins, so that we could see not only nonthermal but also thermal X-ray emission, which might explain the softness of the X-ray spectra observed in J0737 and J1537. The total luminosity from these emission mechanisms is, of course, a small fraction of \dot{E}_A ; it can be described by an equation similar to equation (8) but with an additional factor in its right-hand side, ϵ_{cap} , which is the fraction of intercepted wind particles captured by the B's magnetosphere. Similar to the emission produced by the wind

interaction with the outer magnetosphere (§4.1.1), the X-ray luminosity should decrease with increasing d_{AB} (i.e., it should be lower near apastron) and vanish during the phase intervals when pulsar B is far from the equatorial plane of pulsar A⁵. In addition, the fraction ϵ_{cap} should depend on the angle between the B’s magnetic axis and the line connecting the two pulsars. This may lead to an additional modulation of L_X with the orbital period and the period of pulsar B unless the B’s magnetic axis is perpendicular to the orbital plane, as expected if the main braking mechanism for pulsar B is its interaction with the A’s wind (Arons et al. 2004; Lyutikov 2004). In addition, the X-ray emission caused by the captured wind should show pulsations with the B’s spin period.

There is also an interesting possibility that the wind’s particles that reach the B’s surface and heat the polar caps can facilitate the extraction of electrons or ions from the polar cap surface by the pulsar’s electric field, triggering the pair cascade in pulsar B. In this case, the A’s wind works as a catalyst of B’s X-ray (and possibly radio) emission, providing an additional luminosity associated with the loss of the pulsar B’s spin energy⁶. The orbital phase dependence of this luminosity should be similar to that of the above-discussed captured wind. In particular, even if B is a dead pulsar when no wind blows on it (e.g., when it is far from the A’s equatorial plane), it may become “resurrected” on the orbit segments where it captures the wind.

Quantitative predictions of the properties of the X-ray emission induced by the captured wind are highly uncertain, depending on the unknown wind properties, structure of the magnetic field near the interaction region, etc. We can crudely estimate the number of A’s wind particles captured by B per unit time: $\delta\dot{N}_A = \kappa_A \dot{N}_{\text{GJ},A} \epsilon_{\Omega} \epsilon_{\text{cap}}$, where $\dot{N}_{\text{GJ},A} \sim (3\dot{E}_A c / 2e^2)^{1/2}$ is the Goldreich-Julian rate of particle ejection from the A’s magnetosphere, κ_A the pair production multiplicity, and $\epsilon_{\Omega} \sim f_A(r_B/2d_{AB})^2$. Assuming $r_B < R_{lc,B}$, we obtain $\delta\dot{N}_A \sim 2.2 \times 10^{27} \kappa_A \epsilon_{\text{cap}} (a/d_{AB})^{4/3} P_B^{4/3} (f_A^2 g_B \dot{E}_{B,30})^{1/3} \text{ s}^{-1}$ for J1537, and $\delta\dot{N}_A \sim 4.4 \times 10^{28} \kappa_A \epsilon_{\text{cap}} (f_A^2 g_B)^{1/3} \text{ s}^{-1}$ for J0737. If the captured wind is the only source of X-rays, the product $\kappa_A \epsilon_{\text{cap}}$ should be large enough to provide the observed X-ray luminosity: e.g., $\kappa_A \epsilon_{\text{cap}} > 3 \times 10^3 (f_A^2 g_B)^{-1/3} P_B^{-4/3} \dot{E}_{B,30}^{-1/3} (a/d_{AB})^{-4/3} (10^5 m_e c^2 / \bar{\mathcal{E}})$ in J1537 and $\kappa_A \epsilon_{\text{cap}} > 0.8 \times 10^3 (f_A^2 g_B)^{-1/3} (10^5 m_e c^2 / \bar{\mathcal{E}})$ in J0737, where $\bar{\mathcal{E}}$ is an average energy per captured particle reradiated in X-rays (Zhang & Loeb 2004 assume $\kappa_A \sim 10^6$, $\epsilon_{\text{cap}} \sim 0.1$ in their estimates for J0737; as we have mentioned above, at such large κ_A no X-rays can be expected from the wind that was not captured). For $\kappa_A \sim 10^2$ obtained in standard cascade theory, we have to invoke the above-mentioned activation of pulsar B by the captured wind to explain the observed energetics.

Note that a large value of $\kappa_A \epsilon_{\text{cap}}$ is also required for $\delta\dot{N}_A$ to exceed the intrinsic B’s pair production rate,

⁵ We should mention that such orbital phase dependencies are expected not only for the nonthermal but also for the thermal component because the polar cap cooling time scales are very short (about a few microseconds for $B \sim 10^{12}$ G; e.g., Gil et al. 2003).

⁶ If such a mechanism works, we should expect that \dot{E}_B (and \dot{P}_B) are increased during the “activation phases”.

$\dot{N}_B = \kappa_B \dot{N}_{\text{GJ},B} = 4.4 \times 10^{29} \dot{E}_{B,30}^{1/2} \kappa_B \text{ s}^{-1}$. It occurs when $\kappa_A \epsilon_{\text{cap}} / \kappa_B > 200 (d_{AB}/a)^{4/3} P_B^{-4/3} (f_A^2 g_B)^{-1/3} \dot{E}_{B,30}^{1/6} \text{ s}^{-1}$ and $13 (f_A^2 g_B)^{-1/3}$ for J1537 and J0737, respectively.

Thus, we can conclude that energizing the B’s magnetosphere or heating its surface by the particles from the A’s wind can explain the observed dependence of the X-ray flux on binary phase. However, it would require a rather high pair production multiplicity in pulsar A and considerable anisotropy of the A’s wind.

4.2. X-ray emission from individual pulsars

Since solitary pulsars are known to emit X-rays, at least some fraction of the detected X-rays could come from one or both of the DNSB components, even if the X-ray emission caused by the interaction of the A’s wind with the B’s magnetosphere were negligible. In particular, MSPs can exhibit both nonthermal (magnetospheric) and thermal (polar cap) components in their X-ray spectra, the latter dominating in MSPs with $\dot{E} \lesssim 10^{34} \text{ ergs s}^{-1}$. Typical thermal conversion efficiencies, $\eta_{\text{th}} \equiv L_{\text{bol}} / \dot{E}$, are $(0.3\text{--}3) \times 10^{-4}$ (Zavlin 2006, and references therein). The efficiencies inferred from the BB fits of the J1537 and J0737 spectra, 6.1×10^{-5} and $4.6 \times 10^{-5} (\cos \zeta)^{-1} D_{500}^2$, respectively, are within that range⁷. The polar cap radii derived from the BB fits, are smaller than the conventional PC radii [$r_{\text{pc}} \equiv (2\pi R_{\text{NS}}^3 / cP)^{1/2} = 740 \text{ m}$ and 960 m , respectively], similar to other pulsars (e.g., Zavin & Pavlov 2004; Zavlin 2006). Thus, the luminosities and the soft spectra of J1537 and J0737 are consistent with being emitted from polar caps of J1537A and J0737A, but of course such emission would not show any dependence on binary phase.

The X-ray emission in J1537 might also originate from J1537B if this NS is not a “dead pulsar”, i.e. it is still capable of producing e^+e^- pairs emitting curvature and synchrotron radiation in the magnetosphere and heating its polar caps. Indeed, the X-ray spectrum of J1537 resembles the spectra of old ($\tau \sim 1\text{--}10 \text{ Myr}$) solitary radio pulsars (e.g., PSR B0950+08; Zavlin and Pavlov 2004). However, the J1537’s luminosity (e.g., $L_X = 8.5 \times 10^{28} \text{ ergs s}^{-1}$ in the 1–10 keV band, for the PL fit) is rather high for such an old pulsar⁸; it would either imply a high spin-down luminosity, $\dot{E}_{\text{J1537B}} \gtrsim 10^{32} \text{ ergs s}^{-1}$, or suggest that the X-ray efficiencies of old pulsars strongly grow with decreasing \dot{E} , which is hardly supported by observations (cf. Fig. 5 in Kargaltsev et al. 2006). Moreover, such an interpretation is firmly excluded for J0737, whose X-ray luminosity exceeds $\dot{E}_{\text{J0737B}} = 1.6 \times 10^{30} \text{ ergs s}^{-1}$.

Thus, if the observed J1537’s emission originates from the surface or magnetosphere of one of the binary companions, J1537A is a much more viable candidate than J1537B. The assumption that most of the observed X-ray emission is generated at the polar caps (or magnetosphere) of J1537A would be strongly supported if X-ray

⁷ Since the orientations of the axes is poorly known for J0737A (Demorest et al. 2004; Manchester et al. 2005), the value of $(\cos \zeta)$ is very uncertain.

⁸ Based on the J1537’s proper motion and distance from the Galactic plane, Thorsett et al. (2005) argue that the SN explosion that produced J1537B occurred $\gtrsim 10 \text{ Myrs}$ ago.

pulsations at the J1537A period are found in future observations. An indirect support for this interpretation would also be provided by detection of X-ray pulsations from J0737 at the J0737A's period. On the other hand, confirming the reduced count rate near apastron would virtually rule out this interpretation and put an interesting upper limit on the MSP luminosity.

4.3. Emission from the A's wind interacting with the interstellar medium

The velocities of J1537 and J0737 in the plane of the sky, $v_{\perp} \simeq 120$ and 70 km s⁻¹, respectively, are large enough to assume that these DNSBs are moving through the ISM with supersonic speeds, i.e., $v > c_s = 15 (\mu/0.6)^{-1/2} T_4^{1/2}$ km s⁻¹, where μ and $T = 10^4 T_4$ K are the molecular weight and temperature. At a supersonic speed, the pulsar's wind forms a termination shock (TS) in the ISM. For an isotropic wind, the TS acquires a bullet-like shape (Bucciantini, Amato, & Del Zanna 2005), with a distance $R_h \simeq (\dot{E}_A/4\pi c\rho v^2)^{1/2} = 4.0 \times 10^{15} \dot{E}_{A,33}^{1/2} n^{-1/2} v_7^{-1}$ cm between the pulsar and the bullet head [here $n = \rho/(1.66 \times 10^{-24}$ g) is the ISM number density in atomic mass units per cm³, and v_7 is the pulsar speed in units of 100 km/s]. For large enough $\gamma^2 B$ in the shocked plasma (see equation [6]), it can generate X-rays, as discussed by Granot & Mészáros (2004) for J0737.

The interpretation of the observed X-rays as generated by the A's wind interaction with the ISM rather than with the B's magnetosphere (§4.1) has two apparent advantages for explaining the energetics (but not the putative dependence on binary phase in J1537): a much larger fraction of the A's wind is intercepted (e.g., $\epsilon_{\Omega} \sim 0.5$), and, possibly, a larger fraction of the A's wind energy is carried by particles (ϵ_e is closer to unity) because a larger fraction of the wind's magnetic energy can be converted into particle energy at such large distances, $R_h \gg d_{AB}$. On the other hand, this interpretation may have its own problems, even with the X-ray energetics. First of all, since the wind's magnetic field is much lower at the TS than at the site of interaction with the B's magnetosphere, the synchrotron power and radiative efficiency, ϵ_{rad} , are much lower, which requires much higher particle energies for the radiation to be emitted in the X-ray range. Assuming that the magnetization parameter (i.e., the ratio of the Poynting flux to the kinetic energy flux) is small, $\sigma \ll 1$, we can, following Kennel & Coroniti (1986), estimate the post-shock magnetic field at the shock head: $B \sim 3\sigma^{1/2}(4\pi\rho v^2)^{1/2} = 14\sigma_{-2}^{1/2}n^{1/2}v_7 \mu\text{G}$, where $\sigma_{-2} = \sigma/10^{-2}$. For the synchrotron radiation in such a field to be emitted in the X-ray range, we should have enough electrons in the energy range $\gamma \sim (1-3) \times 10^8 \sigma_{-2}^{-1/4} n^{-1/4} v_7^{-1/2}$. Such energies are too high to be acquired in the pulsar magnetosphere. The wind electrons can be further accelerated in the pre-shock wind by the conversion of the electromagnetic wind's energy into kinetic energy. However, irrespective of the (poorly understood) conversion mechanism, the maximum energy is limited by the value $\gamma_{\text{max}} = (e^2/2m_e c^3)\dot{N}_{\text{GJ},A}\kappa_A^{-1}$ (see Lyubarsky & Kirk 2001), which gives $\gamma_{\text{max}} = 0.9 \times 10^8 \kappa_A^{-1}$ and $1.6 \times 10^8 \kappa_A^{-1}$ for J1537A and J0737A, respectively. These limiting en-

ergies are sufficiently large only at very small multiplicities ($\kappa \lesssim 1$ for reasonable σ , n , and v), much lower than $\kappa \sim 100$ expected from the pulsar models. Too low electron energies and magnetic fields may be responsible for the fact that no TSs around supersonically moving MSPs have been convincingly detected in X-rays (e.g., Zavlin et al. 2002), in contrast to forward bow shocks seen in H α .

It is worth mentioning another problem with the wind-ISM interaction as the source of X-ray emission from close binary pulsars, such as J1537 and J0737. The conventional model for the shock (and the above consideration) assume that the pulsar's velocity relative to ISM is constant. However, a binary pulsar rotates around the center of mass, and the velocity of this motion may even exceed the binary systemic velocity. For instance, the A's orbital velocity varies between 150 and 263 km s⁻¹ in J1537 and between 275 and 328 km s⁻¹ for J0737. This means that both the absolute magnitude and the direction of the A's velocity relative to ISM vary with the orbital period. Moreover, using the pulsar's velocity relative to ISM in the above consideration would result in TS changing its position and orientation in the ISM (e.g., the TS head could appear *behind* the moving binary during some fraction of the binary period). On the other hand, the characteristic time of propagation of perturbations in the ultrarelativistic wind, $\gtrsim R_h/c \sim 30-100$ hours, exceeds the binary period, so that we do not expect the wind-ISM interaction to create a rotating (or wobbling) TS "bullet". Nevertheless, even if this interaction results in a TS whose global properties, averaged over the orbital period, resemble those of a solitary pulsar moving with a constant speed v , this structure should respond to the perturbations caused by the fast binary motion, and these perturbations should manifest themselves in periodic variations in the radiation from the shocked plasma. However, no such variations have been seen in the X-ray radiation from J0737. If future X-ray observations of J0737 put more stringent limit on the orbital variation, it will be an additional argument against the interpretation in terms of the wind-ISM interaction.

5. CONCLUSIONS

We have detected the DNSB J1537 in X-rays, analyzed its X-ray spectrum and light curve, and compared the properties of its X-ray emission with those of the double pulsar J0737. Although the X-ray spectra and luminosities of these systems are similar, J1537 shows a gap in its light curve during an interval of 0.35 of orbital period around apastron while J0737 does not show a significant orbital phase dependence. There are two viable interpretations of the X-ray emission: it can be caused by interaction of the pulsar A's wind with pulsar B (§4.1), including the capture of the wind particles (§4.1.2), or it can be emission from the magnetosphere or, more likely, hot polar caps of pulsar A (similar to solitary MSPs with $\dot{E} < 10^{34}$ ergs s⁻¹; §4.2). The former interpretation can explain the putative orbital phase dependence in J1537 if the A's wind is mostly concentrated in the equatorial plane around the A's spin axis inclined to the orbital plane. The phase dependence can also be associated with the large eccentricity of J1537 (much larger than in J0737) because the X-ray luminosity depends on binary separation. On the contrary, no orbital phase de-

pendence is expected if the X-rays are produced by pulsar A.

Unfortunately, the scarce count statistics does not allow us to discriminate between the different interpretations. Further observations of both J1537 and J0737, which have different orbital parameters and orientations with respect to the observer, should provide a clue to the nature of the X-ray radiation from DNSBs and the properties of pulsars and their winds.

If future observations of J1537 confirm the deficit of X-ray flux during a substantial part of orbit, this would prove that the X-rays are produced via interaction between the binary companions. If a similar deficit is observed at the opposite part of the orbit, it would strongly support the hypothesis that the A's wind is concentrated towards the equatorial plane, and it would allow one to measure the opening angle of the equatorial outflow. If, on the contrary, the X-ray flux shows a maximum at periastron, it would mean that the binary separation is the main cause of the variable X-ray flux. For J0737, the dependence of the X-ray flux on orbital phase should be much weaker due to a smaller angle between the orbital angular momentum and the A's spin or/and the much smaller eccentricity. Confirming the interaction with the B's outer magnetosphere as the source of X-rays would provide strong evidence that the A's wind is accelerated up to energies $\gtrsim 10^6 m_e c^2$ at the interaction site, likely by magnetic reconnection. In such a scenario, one can expect X-ray pulsations with B's period, especially if the wind is captured by pulsar B. If the emission spectrum is found to be softer at the pulsations maxima, we would conclude that a fraction of the captured A's wind is channeled onto B's polar caps, heating them to X-ray temperatures. Detection of radiation caused by the capture of the A's wind would put a stringent lower limit on pair multiplicities in pulsar A.

If future observations rule out any orbital phase de-

pendence in the DNSBs (including the flux deficit near apastron in J1537), but pulsations at the A's period are detected, then we will have to conclude that the X-ray emission is produced by pulsar A itself, while the interaction of the A's wind with pulsar B is insignificant. This would mean that conversion of the intercepted wind's power into X-ray luminosity is inefficient, possibly because the particles are not accelerated to high enough energies (which results in small values of ϵ_X and ϵ_{rad} in eq. [8]). In this case, studying the X-ray spectrum and pulsations would better characterize pulsar A, allowing one to compare its properties with those of "ordinary" MSPs, which have shorter periods and larger characteristic ages.

Finally, it is quite plausible that the observed emission consists of two components: a soft thermal component from pulsar A and a hard nonthermal component from the A's wind interaction with pulsar B, as suggested by the X-ray spectra of J0737 and J1537. If this is the case, we expect to see periodic variations with both the orbital and A's periods. Also, the relative contributions of these two components are expected to vary with orbital phase. The changes can be seen through phase-resolved spectroscopy because the wind emission is expected to be substantially harder than the MSP emission.

To conclude, further deep observations of J1537 and J0737, and perhaps other DNSBs, would be of great interest as they will constrain both the properties of pulsar winds, including their interaction with the neutron star companions, and the properties of pulsars themselves.

We thank Ingrid Stairs for providing the updated ephemeris for J1537 and Firoza Sutaria for the help with the analysis of the *XMM-Newton* data. This research was supported by NASA grants NAG5-10865 and NAS8-01128 and *Chandra* award SV4-74018.

REFERENCES

- Achtenberg, A., Gallant, Y. A., Kirk, J. G., & Guthmann, A. W. 2001, *MNRAS*, 328, 393
- Arons, J., Backer, D. C., Spitkovsky, A., & Kaspi, V. M. 2004, in *Binary Radio Pulsars*, eds. F. A. Rasio & I. H. Stairs, ASP Conf. Ser., in press (astro-ph/0404159)
- Arons, J., & Tavani, M. 1993, *ApJ*, 403, 249
- Bucciantini, N., Amato, L. & del Zanna, L. 2005, *A&A*, 423, 253
- Burgay, M., et al. 2003, *Nature*, 426, 531
- Campana, S., Possenti, A., & Burgay, M. 2004, *ApJ*, 613, L53
- Cash, W. 1979, *ApJ*, 228, 939
- Coles, W. A., McLaughlin, M. A., Rickett, B. J., Lyne, A. G., & Bhat, N. D. R. 2005, *ApJ*, 623, 392
- Demorest, P., Ramachandran, R., Backer, D. C., Ransom, S. M., Kaspi, V., Arons, J., & Spitkovsky, A. 2004, *ApJ*, 615, L137
- Dickey, J. M., & Lockman, F. J. 1990, *ARA&A*, 28, 215
- Gil, J., Melikidze, G. I., & Geppert, U. 2003, *A&A*, 407, 315
- Granot, J., & Mészáros, P., 2004, *ApJ*, 609, L17
- Hibschman, J. A., & Arons, J. 2001, *ApJ*, 560, 871
- Jetet, F. A., & Ransom, S. M. 2004, *Nature*, 428, 919
- Kargaltsev, O. Y., Pavlov, G. G., & Garmire, G. P. 2006, *ApJ*, 636, 406
- Kennel, C. F., & Coroniti, F. V. 1984, *ApJ*, 283, 694
- Kirk, J., & Skjæraasen, O. 2003, *ApJ*, 591, 366
- Konacki, M., Wolszczan, A., & Stairs, I. H. 2003, *ApJ*, 589, 495
- Lyne, A. G., et al. 2004, *Science*, 303, 1153
- Lyutikov, M. 2004, *MNRAS*, 353, 1095
- Lyutikov, M., & Thompson, C. 2005, *ApJ*, 634, 1223
- Manchester, R. N., et al. 2005, *ApJ*, 621, L49
- McLaughlin, M. A., et al. 2004, *ApJ*, 605, L41
- Lyubarsky, Y., & Kirk, J. G. 2001, *ApJ*, 547, 437
- Pellizzoni, A., De Luca, A., Mereghetti, S., Tiengo, A., Mattana, F., Caraveo, P., Tavani, M., & Bignami, G. F. 2004, *ApJ*, 612, L49
- Rafikov, R. R., & Goldreich, P. 2005, *ApJ*, 631, 488
- Stairs, I. H. 2004, *Science*, 304, 547
- Stairs, I. H., Thorsett, S. E., Taylor, J. H., & Wolszczan, A. 2002, *ApJ*, 581, 501
- Stairs, I. H., Thorsett, S. E., & Arzoumanian, Z. 2004, *Phys. Rev. Lett.*, 93, 141101
- Stappers, B. W., Gaensler, B. M., Kaspi, V. M., van der Klis, M., & Lewin, W. H. G. 2003, *Science*, 299, 1372
- Thorsett, S. E., Dewey, R. J., & Stairs, I. H. 2005, *ApJ*, 619, 1036
- Wolszczan, A. 1991, *Nature*, 350, 688
- Zavlin, V. E. 2006, *ApJ*, 638, 951
- Zavlin, V. E., & Pavlov, G. G. 2004, *ApJ*, 616, 452
- Zavlin, V. E., Pavlov, G. G., Sanwal, D., Manchester, R. N., Trümper, J., Halpern, J. P., & Becker, W. 2002, *ApJ*, 569, 894
- Zhang, B., & Loeb, A. 2004, *ApJ*, 614, L53

TABLE 1
OBSERVED AND DERIVED PARAMETERS FOR J1537+1155 AND
J0737-3039 DNSBs

Parameter	J1537+1155	J0737-3039
Binary period, P_b (days).....	0.421	0.102
Relative semimajor axis, a (10^{11} cm)	2.28	0.878
Eccentricity, e	0.274	0.0877
Distance, d (kpc).....	1.0	≈ 0.5
Orbital inclination, $\sin i$	0.975	1.000
Transverse velocity, v_{\perp} (km/s).....	120	70
Mass, M (M_{\odot}).....	2.68	2.59

NOTE. — Based on the data from Stairs et al. (2002, 2004), Konacki et al. (2003), Lyne et al. (2004), Manchester et al. (2005), and Cole et al. (2005). The transverse velocity in the plane of the sky, v_{\perp} , is uncorrected for the solar system motion.

TABLE 2
OBSERVED AND DERIVED PARAMETERS FOR J1537+1155A, J0737-3039A AND J0737-3039B PULSARS.

Parameter	J1537+1155A	J0737-3039A	J0737-3039B
Spin period, P (ms).....	37.90	22.70	2773.46
Period derivative, \dot{P} (10^{-17}).....	0.242	0.174	88
Dispersion measure, DM (cm^{-3} pc) ...	11.6	48.9	48.7
Angle δ (deg)	25 ± 4 (or 155 ± 4)	$0 - 60$ (or $120 - 180$)	...
Angle α (deg)	103	$0 - 60$...
Mass (M_{\odot})	1.33	1.34	1.25
Semimajor axis, a (10^{11} cm)	1.12	0.424	0.454
Surface magnetic field, B_s (10^{10} G)....	0.97	0.64	158
Spin-down power, \dot{E} (10^{33} erg s^{-1})....	1.8	5.8	0.0016
Age, $\tau = P/(2\dot{P})$, (Myr).....	248	210	50
Light cylinder radius, R_{lc} (10^8 cm) ...	1.8	1.1	130
Magnetic field at R_{lc} , B_{lc} (G)	1660	5050	0.69
Polar cap radius, R_{pc} (m)	740	960	87
Primary pair flux, \dot{N}_{GJ} (10^{30} s^{-1}).....	19	34	0.6

NOTE. — Based on the data from Stairs et al. (2002, 2004), Lyne et al. (2004), and Manchester et al. (2005). Angle δ is between the pulsar's spin and orbital rotation axis. Angle α is between the pulsar's spin and magnetic axis. The surface magnetic field, B_s , is assumed to be that of a dipole and given at the equator.

TABLE 3
PARAMETERS OF PL AND BB MODELS FITTED TO THE *Chandra* AND XMM-NEWTON SPECTRA OF J1537 AND J0737

Instrument	Model	$N_{H,20}$ ^a	Norm. ^b	Γ or kT ^c	C/dof	Q ^d	L_X or $L_{bol}(\cos \zeta)$ ^e
J1537+1155							
ACIS	PL	3.6	$5.7^{+1.6}_{-1.5} \times 10^{-7}$	$3.17^{+0.52}_{-0.52}$	1.1/2	12%	$6.1^{+3.0}_{-2.0} \times 10^{29}$
ACIS	BB	3.6	$4.8^{+3.5}_{-3.0} \times 10^7$	193^{+37}_{-30}	5.3/2	76%	$6.8^{+2.1}_{-2.1} \times 10^{28}$
J0737-3039							
ACIS	PL	5.0	$1.01^{+0.14}_{-0.16} \times 10^{-5}$	$2.93^{+0.29}_{-0.31}$	1.7/4	5%	$2.27^{+0.42}_{-0.39} \times 10^{30}$
ACIS	BB	5.0	$1.91^{+0.99}_{-0.71} \times 10^8$	192^{+17}_{-15}	5.7/4	52%	$2.67^{+0.33}_{-0.37} \times 10^{29}$
MOS1+2	PL	5.0	$0.98^{+0.08}_{-0.10} \times 10^{-5}$	$3.35^{+0.19}_{-0.19}$	10.0/14	12%	$3.03^{+0.50}_{-0.49} \times 10^{30}$
MOS1+2	BB	5.0	$3.95^{+1.5}_{-1.0} \times 10^8$	169^{+11}_{-13}	16.9/14	62%	$3.28^{+0.40}_{-0.38} \times 10^{29}$

NOTE. — The errors are at the 68% confidence level for one interesting parameter.

^aFixed values of hydrogen column density, in units of 10^{20} cm^{-2} .

^bNormalization: Spectral flux in photons cm^{-2} s^{-1} keV^{-1} at 1 keV or projected area of the emitting region in cm^2 , for the PL and BB models, respectively.

^cPhoton index or BB temperature in eV.

^dPercentage of 10,000 Monte Carlo simulations, drawn from the best-fit model, which give a C-statistic value lower than the best-fit value. Although the BB fits are formally worse than the PL fits, they are statistically acceptable.

^e L_X is the unabsorbed PL luminosity in the 0.2–10 keV band, L_{bol} the bolometric luminosity for the BB fits.